CRYSTAL TO NON EQUILIBRIUM PHASE TRANSITION INDUCED BY BALL-MILLING IN SILICON AND THE IMMISCIBLE Si (Sn, Zn) SYSTEMS

E. Gaffet, Mireille L. Harmelin-Vivien

COLLOQUE DE PHYSIQUE
Colloque C4, supplément au n°14, Tome 51, 15 juillet 1990

CRYSTAL TO NON EQUILIBRIUM PHASE TRANSITION INDUCED BY BALL-MILLING IN SILICON AND THE IMMISCIBLE Si(Sn, Zn) SYSTEMS

E. GAFFET and M. HARMELIN

Centre d'Etudes de Chimie Métallurgique, CNRS, 15, Rue G. Urbain, F-94407 Vitry sur Seine Cedex, France

Résumé - La formation de phases métastables - système pur Si, systèmes non miscibles SiSn, SiZn - (soient : phases amorphes, solutions solides crystallines sursaturées et/ou composés métastables) par chocs mécaniques (broyage) a été mise en évidence par diffraction de RX, des observations par MEB, des analyses chimiques EDX/MEB et enfin la stabilité thermique de ces phases a été étudiée par calorimétrie différentielle à balayage. L'obtention de ces phases indique qu'une réaction de mélange négative n'est pas une condition nécessaire pour la formation d'amorphe sous broyage : le mécanisme de transition de phase doit être distinct de celui mis en jeu lors de l'amorphisation par diffusion de multicouches.

Abstract - Based on XRD patterns, SEM observations, EDX/SEM analyses and DSC experiments, we report on the crystal to metastable phase (i.e. amorphous phases, supersaturated crystalline solid solutions and/or non equilibrium compounds) transition induced by ball - milling in a pure element - a Si powder and in two immiscible binary alloys - Si/Sn and Si/Zn. The observations of such dynamic phase equilibria support the idea that a negative heat of mixing is not a necessary condition for the ball - milling amorphisation : the phase transition mechanism which is induced during ball - milling is different by solid state diffusion of multilayered films.

1 - INTRODUCTION

Amorphous phase formation by mechanical alloying was first reported by A. Y. Yermakov et al /1/ and C.C. Koch /2/ for the Co - Y and Ni - Nb systems respectively. Subsequently such an amorphization process has been observed in many other binary alloy systems, starting from elemental crystalline powders, e.g., Fe - Zr /3/, Ni - Zr /4 - 6/, Ti - Pd /7/, Ni - Ti, Co - Ti, Fe - Ti /8 -10/, Ti - Cu /11/, Co - Sn /12/, or from a mixture of intermetallic compounds in the Ni - Zr system /13 - 15/. Amorphization by M.A. is usually obtained in the case of binary alloys exhibiting a large negative heat of mixing and for which one of the elements is a fast diffuser /16/.
In this paper, we report on the crystal to metastable phase (i.e. amorphous phases, supersaturated solid solutions and/or non equilibrium compounds) transition induced by ball - milling in a pure element - a Si powder and in two immiscible alloys - Si/Sn and Si/Zn. The morphological, structural and the thermal stability of the ball milled powder have been investigated by means of SEM/EDX observations, XRD pattern and DSC experiments

2 - EXPERIMENTAL PROCEDURE

2.1 - BALL - MILLING CONDITIONS

2.1.1 - Si ball - milling - 10 g of pure Si (Hyperpure Polycrystalline Silicon from Wacker Chemitronic - Gmbh - 300 Ωcm n and 3000 Ωcm p) are introduced in a cylindrical tempered steel (12%Cr, 2%C) container of capacity 45 ml. This procedure occurs in a glove box filled with purified argon. Each container is loaded with five steel balls 1.5 cm in diameter and 14g in mass. As the containers are sealed in the glove box with a Teflon O - ring, the milling has been proceeded in stationary argon.Ball milling is carried out using two FRITSCH planetary high energy BM equipments (Pulverisette P7/2 and P5/2). For the last machine, two intensity settings are chosen which are mentioned later as P5/2(10) and P5/2(5). The different ball - milling conditions will be referred hereafter as Si(a), Si(b), Si(c) for the P7/2, P5/2(10), P5/2(5). The higher energetic conditions correspond to Si(a), the lower ones are related to Si(c). The durations of the continuous milling processes have been 95 hours, 70 hours, 96 hours for Si(a), Si(b) and Si(c) respectively.

2.1.2 - Si/Sn And Si/Zn ball milling - As the Sn and Zn particles highly stick to the container walls, only the Si - rich side (Si - Sn) and (Si - Zn) phase diagrams (Fig.1 a and b) have been investigated.

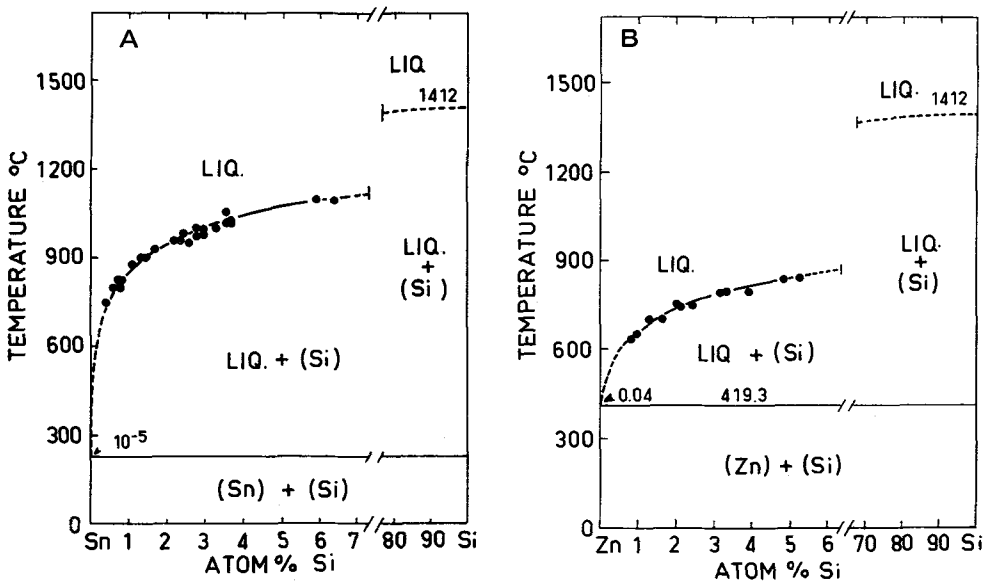

Fig. 1 - Phase diagrams - a) Si-Sn binary alloy, b) Si - Zn binary alloy - (from "The handbook of Binary Phase Diagram - W.G. Moffat - Genium Publishing Corporation - USA)

Two mixing methods have been chosen in order to obtain the composition range
i) - hereafter refered as $\mathbf{Si_x - Sn_{1-x}}$ (I) and $\mathbf{Si_x - Zn_{1-x}}$ (I), - Table 1- , pure Si pieces and pure Sn powder (Prolabo) - pure Zn pieces (Rhone - Poulenc) - are introduced in a cylindrical tempered steel container of capacity 45 ml. This procedure occurs in a glove box filled with purified argon.

ii) - hereafter refered as Si_xSn_{1-x} (II) and Si_x - Zn_{1-x} (II), -Table 1 -, 10 g of Si are first introduced in the container and ball - milled during 72 hours in static argon. Then, the Sn powder (Zn pieces) is introduced and the ball milling is achieved during 96 hours. All the Sn (Zn) recharging sequences are performed in a glove box. Each container is loaded with five steel balls 1.5 cm in diameter and 14g in mass. As the containers are sealed in the glove box with a Teflon O - ring, the milling has been proceeded in stationary argon. Ball milling is carried out using a FRITSCH planetary high energy BM equipment (Pulverisette P5/2 - intensity setting = 10). The durations of the continuous milling processes are listed in Table 1

2.2 - SEM AND EDX/SEM - The particle morphology has been characterized using a Digital Scanning Electron Microscope (Zeiss DSM 950 - SEI mode - Fig 2a, b, c).

The container contamination which may occur during the friction of the particles on the balls and the walls of the container has been determined by SEM/EDX analyses (Si - Li detector from TRACOR).

A semi - quantitative program with internal references (SQ from TRACOR) has been used to analyze the EDX spectra. The chemical analyses are listed in Table 1.

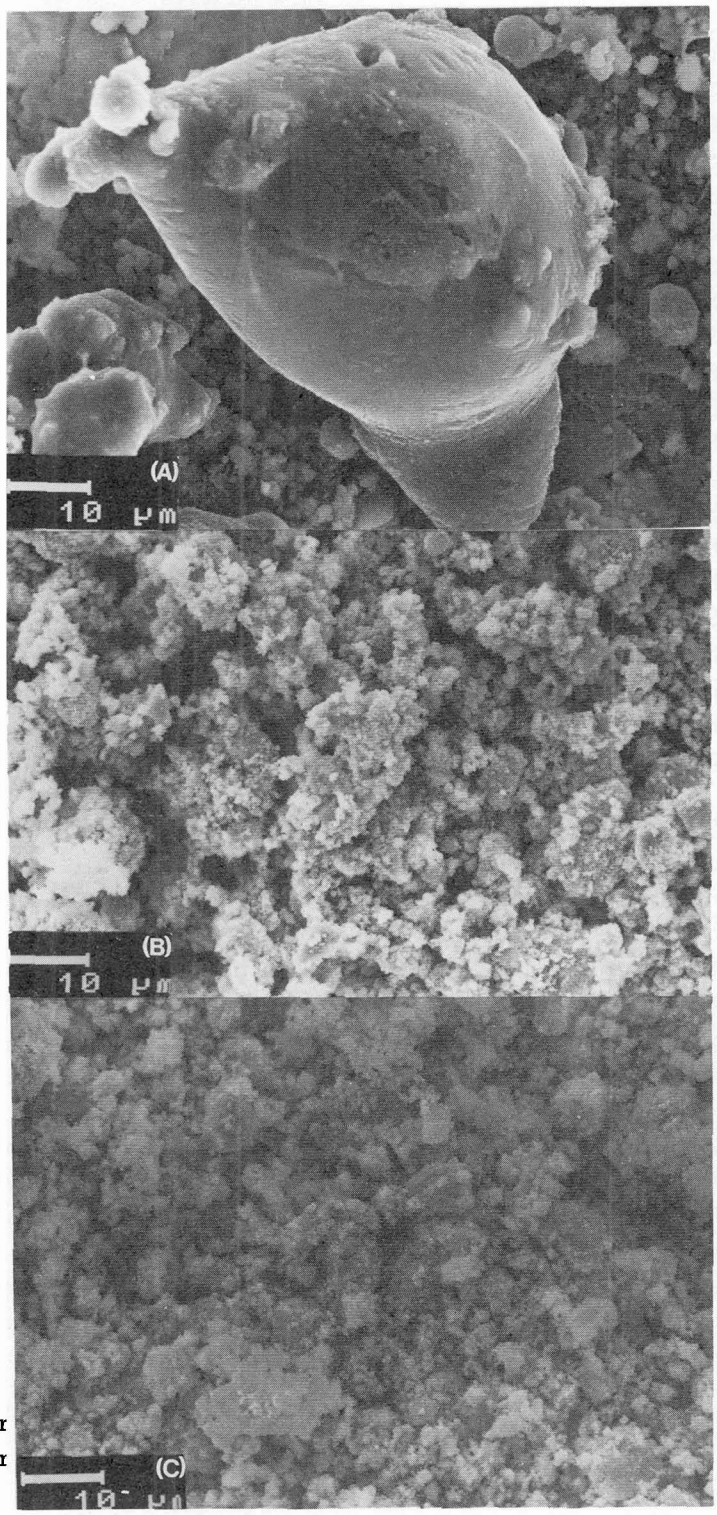

Fig. 2 : a) BM Si powder
b) Typical BM Si-Sn powder
c) Typical BM Si-Zn powder

Table 1 : List of the various experimental conditions and the end - product composition.(%At.) $Si_x Sn_{1-x}$(I) and $Si_x Sn_{1-x}$(II), $Si_x Zn_{1-x}$(I) and $Si_x Zn_{1-x}$(II) see the text (n.d. ≤ 0.05 %At.)

Composition		BM duration	End product composition	
Si(I)				Fe ≤ 0.1, Cr ≤ 0.1
Si(II)				Fe ≤ 0.1, Cr ≤ 0.1
Si(III)				Fe ≤ 0.1, Cr n.d.
$Si_{95}Sn_5$(I)	8.1g Si + 1.9 g Sn	65H	$Si_{95.2\pm0.4}$ - $Sn_{4.8\pm0.4}$	Fe ≤ 0.5, Cr ≤ 0.1
$Si_{95}Sn_5$(II)	10g Si + 2.35g Sn	72+ 96H	$Si_{93.2\pm0.4}$ - $Sn_{6.8\pm0.4}$	Fe ≤ 2.0, Cr ≤ 0.1
$Si_{90}Sn_{10}$(I)	7.0g Si + 3.0 g Sn	96H	$Si_{97.2\pm0.2}$ - $Sn_{2.8\pm0.2}$	Fe ≤ 0.3, Cr≤ 0.1
$Si_{90}Sn_{10}$(II)	10.0g Si + 4.3g Sn	60H + 96H	$Si_{98.1\pm0.3}$ - $Sn_{1.9\pm0.1}$	Fe ≤ 0.3, Cr ≤ 0.1
$Si_{80}Sn_{20}$(I)	5.0g Si + 5g Sn	96H	$Si_{96.1\pm0.2}$ - $Sn_{3.9\pm0.2}$	Fe ≤ 0.7, Cr ≤ 0.1
$Si_{80}Sn_{20}$(II)	10.0gSi + 10.0g Sn	60H + 96H	$Si_{94.2\pm0.3}$ - $Sn_{5.8\pm0.3}$	Fe ≤ 3.5, Cr ≤ 0.5
$Si_{70}Sn_{30}$(I)	3.6g Si + 6.4g Sn	96H	$Si_{72.0\pm3.0}$ - $Sn_{28.0\pm3.0}$	Fe ≤ 3.5, Cr ≤ 0.5
$Si_{70}Sn_{30}$(II)	10g Si + 17.8 g Sn	72H + 96H	$Si_{75.3\pm3.0}$ - $Sn_{24.7\pm3.0}$	Fe ≤ 1.0, Cr ≤ 0.5
$Si_{95}Zn_5$(I)	8.9g Si + 1.1g Zn	96H	$Si_{89.0\pm1.0}$ - $Zn_{11.0\pm1.0}$	Fe ≤ 2.0, Cr≤ 0.5
$Si_{95}Zn_5$(II)	10g Si + 1.15 g Zn	60H + 96H	$Si_{95.1\pm0.8}$ - $Zn_{4.9\pm0.8}$	Fe ≤ 0.2, Cr n.d
$Si_{90}Zn_{10}$(I)	8g Si + 2g Zn	140H	$Si_{84.8\pm6.0}$ - $Zn_{15.2\pm6.0}$	Fe ≤ 3.0, Cr ≤ 0.5
$Si_{90}Zn_{10}$(II)	10g Si + 2.55 g Zn	72H + 144H	$Si_{85.0\pm3.0}$ - $Zn_{15.0\pm3.0}$	Fe ≤ 0.5, Cr ≤ 0.1
$Si_{80}Zn_{20}$(I)	6.3g Si + 3.71g Zn	140H	$Si_{76.5\pm8.0}$ - $Zn_{23.5\pm8.0}$	Fe ≤ 3.0, Cr ≤0.5
$Si_{80}Zn_{20}$(II)	10g Si + 5.90 g Zn	72H + 144H	$Si_{74.0\pm6.0}$ - $Zn_{26.0\pm6.0}$	Fe ≤ 3.0, Cr ≤ 0.5
$Si_{70}Zn_{30}$(I)	5g Si + 5g Zn	96H	$Si_{52.5\pm7.0}$ - $Zn_{47.5\pm7.0}$	Fe ≤ 1.0, Cr ≤ 0.5
$Si_{70}Zn_{30}$(II)	10 g Si+ 10 g Zn	60H + 96H	$Si_{76.0\pm4.0}$ - $Zn_{24.0\pm4.0}$	Fe ≤ 0.5, Cr ≤ 0.1

2.3 - X - RAY INVESTIGATIONS - The X - ray diffraction patterns of the BM powders have been obtained using a (θ - 2θ) PHILIPS diffractometer with CoK_α radiation (λ = 0.17889 nm). A numerical method has been used in order to analyze the X - Ray diffraction patterns and to obtain the position and the full-width at half height of the various peak (For details see /17, 18/).The Bragg expression has been applied to determine the d parameter corresponding to the diffraction peak position (θ): $\lambda = 2\, d \sin\theta$. The effective diameter of the particles (hereafter refered as Φ) has been calculated from the Scherrer expression :$\Phi = 0.91\ \lambda / (B \cos\theta)$ where λ is the X - ray wavelength, B the linewidth (expressed in 2 θ)and θ the diffraction angle

2.3.1 BM Si XRD patterns - Fig 3a, 3b and 3c exhibit the various X - ray diffraction patterns which have been obtained for Si (a), Si(b), Si(c) respectively. Applying the Scherrer formula to the best fit which may be obtained by the ABFfit program (see /17,18/) leads to a mixture of microcrystallites, nanocrystallites and an amorphous phase. Such a classification appears to be schematic since, but with the ABFfit program deconvolution, it is not possible to introduce a continuous variation of the effective size of the particles. Nevertheless, it qualitatively gives the range of the effective diameters of the Si particles (see Table 2).

Table 2 - Effective diameter range of the BM Si crystallites which are in equilibrium with the Si amorphous phase (a_{Si} = 5.43 10^{-1} nm from /19/, a_i in nm).

$\Phi \approx 4$ nm $a_1 = (0.5435 \pm 0.0015)$

Si(a) $\Phi \approx 10$ nm : $a_2 = (0.5425 \pm 0.0015)$

$(a_1 - a_2) / a_2 \approx 0.2\%$

$\Phi \approx 4$ nm : $a_1 = (0.5435 \pm 0.0020)$

Si(b) $\Phi \approx 10$ nm : $a_2 = (0.5430 \pm 0.0020)$

$(a_1 - a_2) / a_2 \approx 0.1\%$

Si(c) $\Phi \approx 8$ nm : $a = (0.5430 \pm 0.0025)$

$(a_1 - a_{Si}) / a_{Si} \approx 0\ \%$

2.3.2 - Si/Sn and Si/Zn XRD pattern - The results of the ABFfit deconvolution of the XRD patterns (Fig. 4 and 5) corresponding to the Si/Sn and Si/Zn BM powder are listed in Table 4.

BM Si/Sn powders : Three phases are detected, a Si(Sn) crystalline solid solution, Sn(Si) phase and an amorphous phase (or a new tetragonal crystalline one). The Si crystalline phase exhibits a strong increase of the diamond cubic parameter as well as the Sn tetragonal crystalline lattice parameters. The c parameter exhibits a larger increase than the a one for the latter phase. For the Sn richer side of the experimented composition, no more amorphous phase has been detected but a new tetragonal phase has been identified with lattice parameters which are strongly different from the pure Sn one.

BM Si/Zn powders : Two crystalline phases and an amorphous phase have been detected for all the compositions which have investigated. The both crystalline phases exhibit an increase of the lattice parameters as compared with the pure Si and Zn elements.

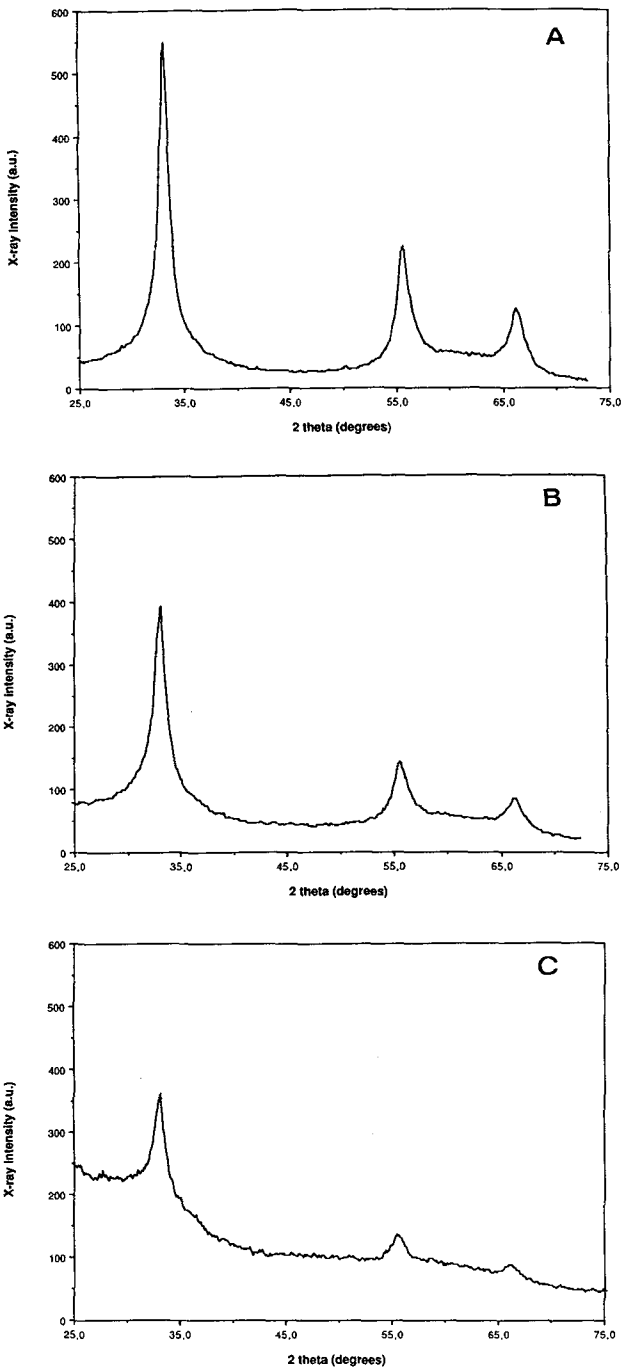

Fig. 3 : X- ray diffraction patterns of the BM Si powders corresponding to the various ball milling conditions : a) P7/2, b) P5/2(10), c) P5/2(5)

Fig. 4. - X - ray diffraction patterns of the ball - milled Si - Sn powders. - a) $Si_{95}Sn_5$*, b) $Si_{90}Sn_{10}$*, c) $Si_{80}Sn_{20}$*, d) $Si_{70}Sn_{30}$*, e) $Si_{95}Sn_5$**, f) $Si_{90}Sn_{10}$**, g) $Si_{80}Sn_{20}$**, h) $Si_{70}Sn_{30}$**

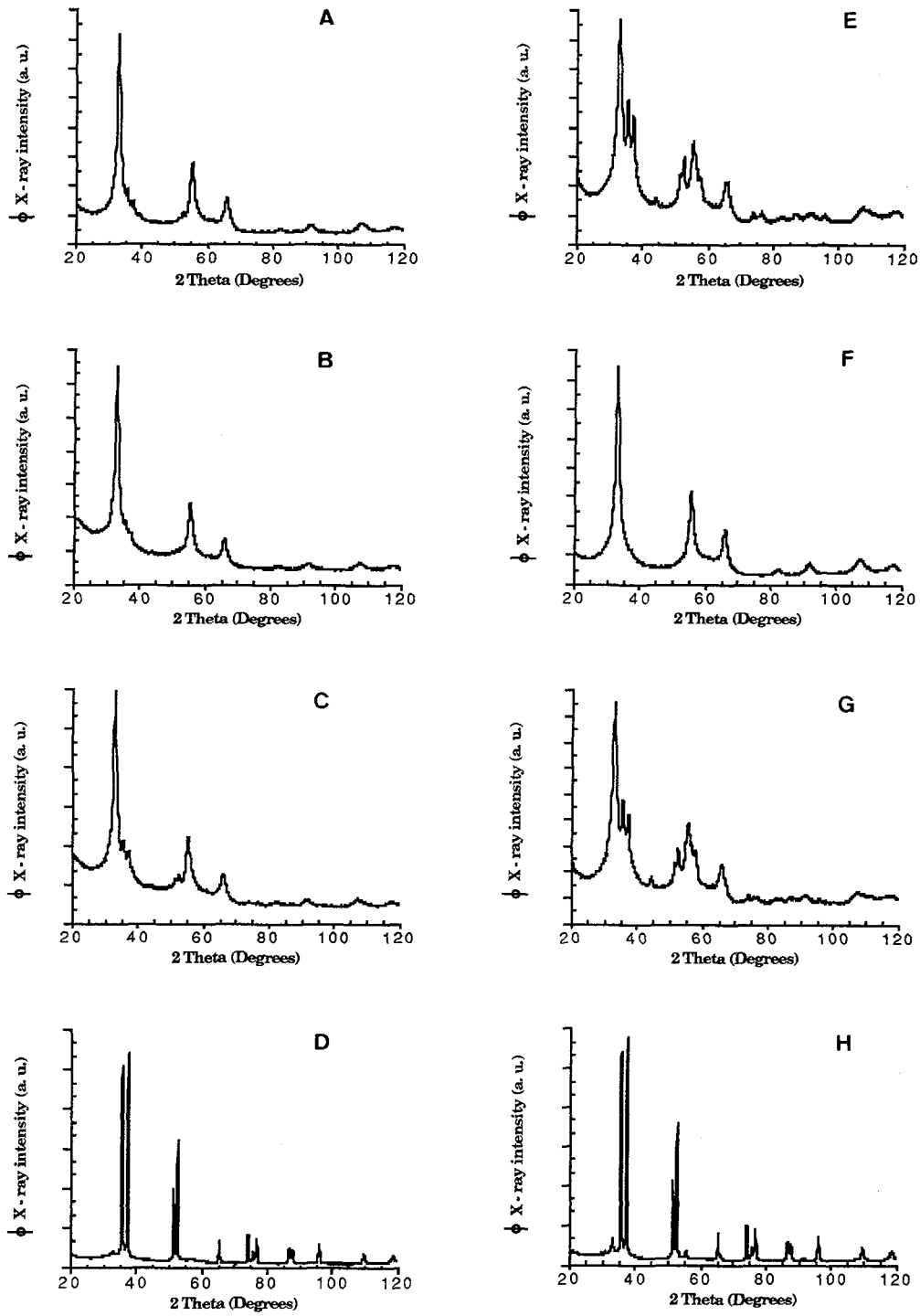

Fig. 5. - X - ray diffraction patterns of the ball - milled Si - Zn powders. - a) $Si_{95}Zn_5$*, b) $Si_{90}Zn_{10}$*, c) $Si_{80}Zn_{20}$*, d) $Si_{70}Zn_{30}$*, e) $Si_{95}Zn_5$**, f) $Si_{90}Zn_{10}$**, g) $Si_{80}Zn_{20}$**, h) $Si_{70}Zn_{30}$**

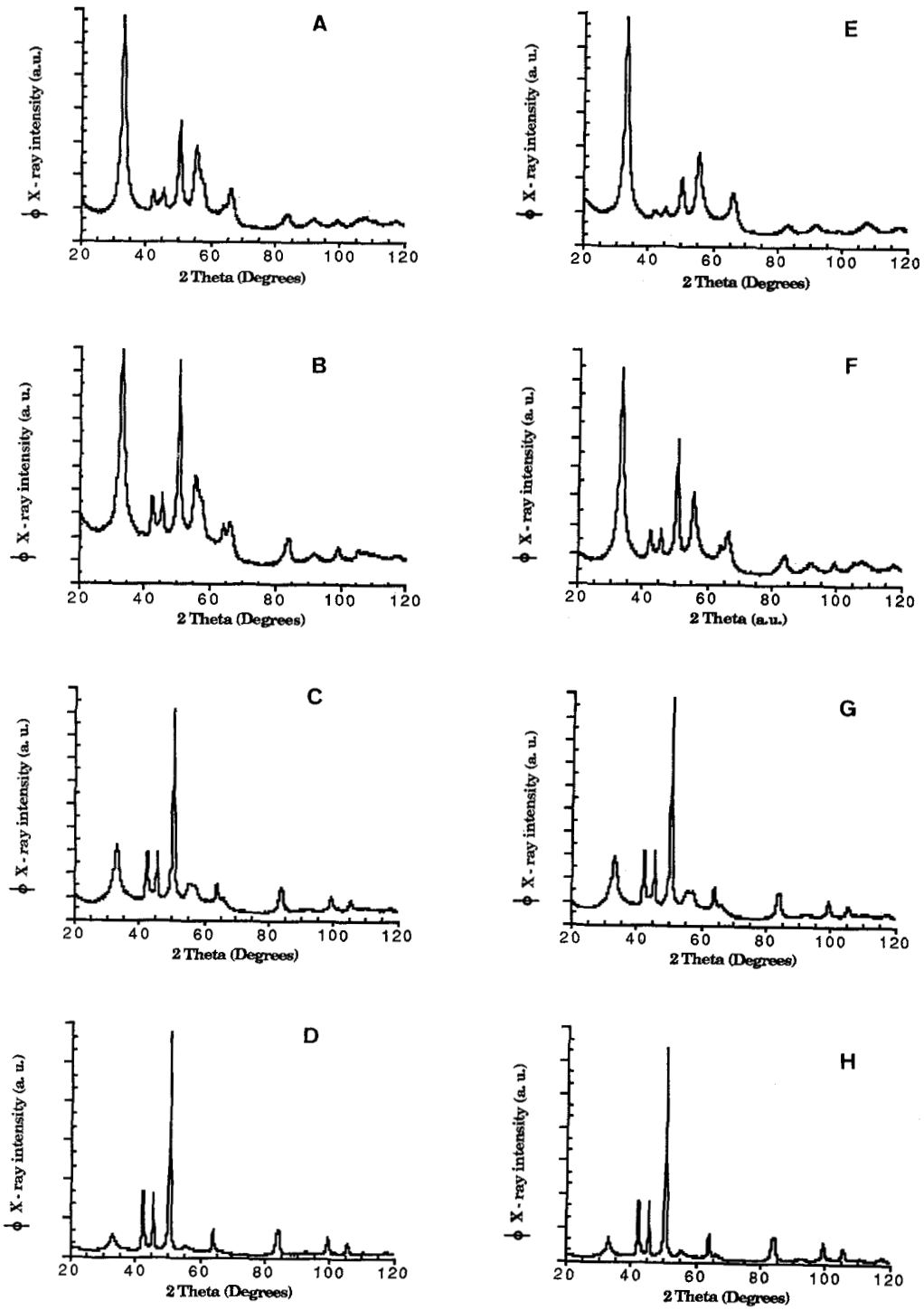

Table 3 - The amorphous phase parameter (d) and Si phase crystalline parameter (a) as a function of the initial compositions and the ball - milling conditions for the Si(Sn/Zn) system.

Si_xSn_{1-x} % at.	a $Si^X(\Delta a/a_{Si})$ 10^{-1} nm	d Am. Phase 10^{-1} nm	a, c $^X(\Delta a/a_{Sn/Zn})$, $(\Delta c/c_{Sn/Zn})$ 10^{-1} nm
Si	a_{Si}= 5.43 /19/		
BM Si		3.16±0.02 /17/	
Sn			a_{Sn} = 5.831
			c_{Sn} = 3.182 / /
$Si_{95}Sn_5$*	5.48 (+0.9)	3.10 (7.5)	a = 5.846 (+0.3)
	5.45 (+ 0.4)		c = 3.196 (+ 0.5)
$Si_{95}Sn_5$**	5.50 (+ 1.3)	3.051 (7.6)	a = 5.846 (+ 0.3)
	5.45 (+ 0.4)		c = 3.199 (+ 0.5)
$Si_{90}Sn_{10}$*	5.48 (+ 0.9)	3.127 (7.6)	a = 5.844 (+ 0.2)
	5.45 (+ 0.4)		c = 3.192 (+ 0.3)
$Si_{90}Sn_{10}$**	5.64 (+ 3.9)	3.148 (5.8)	?
	5.44 (+ 0.3)		
$Si_{80}Sn_{20}$*	5.48 (+ 0.9)	3.100 (7.6)	a = 5.839 (+ 0.1)
	5.45 (+ 0.4)		c = 3.195 (+ 0.4)
$Si_{80}Sn_{20}$**	5.64 (+3.9)	3.036 (7.3)	a = 5.843 (+ 0.2)
	5.46 (+ 0.5)		c = 3.195 (+ 0.4)
$Si_{70}Sn_{30}$*	5.80 (+6.8)	a" = 5.75 (- 1.5)	a = 5.843 (+ 0.2)
	5.47 (+0.7)	c" = 2.79 (- 12.3)	c = 3.188 (+0.2)
$Si_{70}Sn_{30}$**	5.53 (+ 1.8)	a" = 5.72 (- 1.8)	a = 5.844 (+ 0.2)
	5.45 (+ 0.4)	c" = 2.97 (- 6.6)	c = 3.188 (+ 0.2)
Zn			a_{Zn} = 2.665
			c_{Zn} = 4.947 / /
$Si_{95}Zn_5$*	5.46 (+ 0.6)	3.140 (5.7)	a = 2.674 (+ 0.3)
	5.44 (+ 0.2)		c = 4.970 (+ 0.6)
$Si_{95}Zn_5$**	5.46 (+ 0.6)	3.146 (5.7)	a = 2.679 (+ 0.5)
	5.44 (+ 0.1)		c = 4.977 (+ 0.6)
$Si_{90}Zn_{10}$*	5.46 (+0.6)	3.152 (5.6)	a = 2.672 (+ 0.3)
	5.44 (+ 0.1)		c = 4.955 (+ 0.2)
$Si_{90}Zn_{10}$**	5.47 (+ 0.7)	3.139 (6.5)	a = 2.670 (+ 0.2)
	5.44 (+ 0.1)		c = 4.955 (+ 0.2)
$Si_{80}Zn_{20}$*	5.46 (+ 0.6)	3.145 (5.9)	a = 2.671 (+ 0.2)
	5.44 (+ 0.1)		c = 4.948 (+ 0.0)
$Si_{80}Zn_{20}$**	5.47 (+ 0.7)	3.144 (6.0)	a = 2.672 (+ 0.3)
	5.44 (+ 0.2)		c = 4.951 (+ 0.1)
$Si_{70}Zn_{30}$*	5.47 (+ 0.7)	3.144 (5.6)	a = 2.670 (+ 0.2)
	5.45 (+ 0.3)		c = 4.946 (+ 0.0)
$Si_{70}Zn_{30}$**	5.45 (+0.3)	3.136 (5.9)	a = 2.670 (+ 0.2)
			c = 4.950 (+ 0.1)

a", c" No amorphous phase but a crystalline phase with a tetragonal structure.

2.4 - TRANSMISSION ELECTRON MICROSCOPY - Fig. 5 exhibits a typical selected area diffraction pattern on which the typical microcrystalline structure is revealed. Furthermore, in spite of the fact that the rings corresponding to the [220] and [311] indexations exhibit some clear spots, the first ring exhibit a continuous diffuse intensity. This may be explained by an overlap of different contributions. Indeed, as shown by the X - ray diffraction pattern study, the first ring corresponding to the first distance [111] in Si has several contributions : two (at least) crystalline contributions plus the first diffuse halo corresponding to the presence of the amorphous phase. Such an overlap will lead to a continuous diffuse intensity for the first ring.Furthermore between the [220] and [311] rings, a diffuse intensity is observed (indicated by an arrow). It corresponds to the second diffuse peak (second shoulder) of the amorphous phase. Then such an electron diffraction pattern is in good agreement with the previous analyses of the X - ray diffraction patterns.

As the diameter of the selected area is about the micrometer scale, we may affirm that the both structures - crystalline (microcrystalline and/or nanocrystalline) and amorphous phase coexist at the micrometer scale.

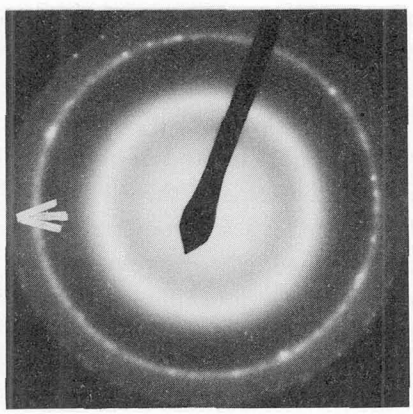

Fig. 5. - Typical SAD pattern obtained from the ball milled Si powder.

2.5. - CALORIMETRIC MEASUREMENTS - The thermal analysis have been carried out using a DSC - 2C PERKIN ELMER. 20 mg sample were sealed in a copper capsule and heated from 50°C to 725°C on flowing pure argon.

Fig. 6 exhibits a typical DSC trace corresponding to the thermal response of Si(c).

Such a thermal response may be analyzed as a low temperature exothermic contribution, followed by an endothermic peak at intermediate temperature and a high temperature exothermic event.

Fig. 6 : DSC traces of Si(c) at heating rate of 2.5°C min-1 (for details see /17/)

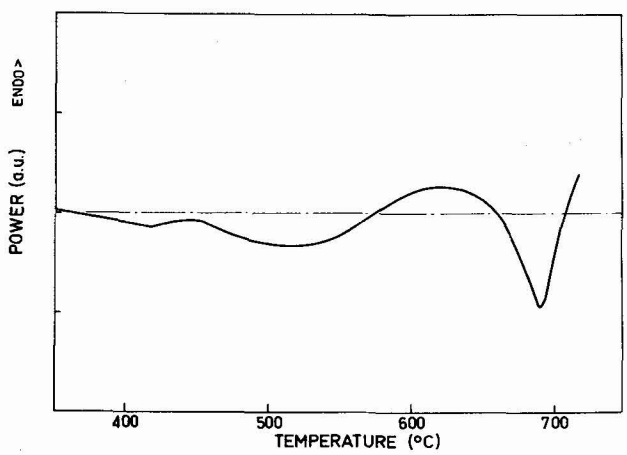

The crystallization peak position is 694°C and 720°C for heating rates of 2.5 °C/min. and 10 °C/min. respectively.The activation energy of the Si amorphous phase crystallisation has been

determined by the Kissinger method /20/ and is equal to 323 $kJmol^{-1}$(or 3.35 $eVat^{-1}$) /17/. Further investigations have to be performed in order to compare the thermal response of the binary alloys with the BM Si powder.

3 - DISCUSSION

3.1 - BALL - MILLED SI POWDER - The above experimental results lead to the existence of a dynamic equilibrium between amorphous Si - phase and polycrystalline Si - phase induced by ball - milling. Other techniques lead to the obtention of a Si amorphous phase, vapor deposition [21], LASER surface treatment [22] or ion irradiation with 1.8 MeV krypton ions [23]. Nevertheless, such techniques only lead to the formation of a thin film (vapor deposition) or just modify a thin thickness of the exposed surface of the material (LASER and/or ion irradiation). Further investigations and better knowledges of the mechanism of the phase transition may lead to the obtention of a three - dimensional amorphous Si phase by ball - milling.Notice that the value of the lattice parameter corresponding to the larger particle size (a_2) is in agreement with that obtained by H. Kiendl : a_{Si} = 0. 54310 nm [19], the lattice parameter corresponding to the lower particle size exhibits a relative difference of 0.2 % for Si (I), 0.1% for Si (II). S. Veprek et al [21] studied the formation of amorphous silicon during condensation from the vaporous phase and determined a critical grain size (depending on the stress deposition conditions) below which the crystalline structure becomes unstable. According to their results, the critical particle size and the corresponding lattice expansion at which the diamond lattice becomes unstable with respect to the amorphous phase under the ball - milling conditions which have been used in our experiments, can be estimated to be :

Si(a)	Φc = 4 nm	$\Delta a_c \approx$ 0.2%
Si(b)	Φc = 4 nm	$\Delta a_c \approx$ 0.1%
Si(c)	Φc = 8 nm	$\Delta a_c \approx$ 0.0 %

Therefore, the crystal to amorphous phase transition may be explained by a refinement of the grain size of the particle which leads to a destabilization of the diamond structure, the critical size of the particle seems to be affected by the ball - milling conditions and the Δa_c value shows a strong correlation with the latter : the higher the energy input during the ball - milling, the larger the value of Δa_c.

Now, let us consider about the thermal behavior during the DSC experiments. Notice that the same kind of the various contributions, i.e. a low temperature exothermic peak, an intermediate temperature endothermic peak and a high temperature exothermic crystallization event have been also encountered for the Ni - Zr system /15/. In the just mentioned work, the origin of the various peaks have been interpreted as a relaxation of the stressed intermetallic compounds (exothermic contribution), followed by a local equilibration between the amorphous phases and the in - situ relaxed compounds leading to a change in composition of the amorphous phases (endothermic effect since the heat of mixing is negative), and at higher temperature, the crystallization of the various amorphous phases (exothermic events). Such an interpretation for the both exothermic contributions which are obtained for the ball - milled Si thermal analysis is also consistent. In the present work, considering that the (Fe - Cr) contamination is very minor, the Si powder behaves as a pure element. Thus, for explaining the intermediate temperature endothermic contribution, we propose to replace the composition

parameter which may be considered as one of the components of the configuration space by another parameter - which remains to be determined - but which may be the configuration space distribution of the Si atoms - in the amorphous state - in dynamic equilibrium with the crystals.

3.2 - BM SI/SN AND SI/ZN POWDERS - The XRD patterns analyses have revealed the simultaneous presence of two crystalline phase and and amorphous phase. As the crystalline phases exhibit the same structure as the pure elemental one but with an increase in the lattice parameters, we may propose that an extension of the solubility have been obtained by the ball - milling process leading to the formation of such supersaturated crystalline solid solution. R. Birringer et al. /24/ have demonstrated the influence of the crystal grain size on the solubility of some elements : the solute solubility of the nanocrystalline materials may be several orders of magnitude larger than in the case of the single crystals : the solubility of Bi (at 373K) in the nanocrystalline Cu grains (10 nm crystal size) was 4% and $<10^{-4}$% in the Cu single crystals. Such a similar effect may be proposed to explain the variation of the crystalline lattice parameter. A so large solute content may also explain the formation of the amorphous phase which may be due to a chemical supersaturation instability of the crystalline lattice.

4 - CONCLUSION

Based on experimental investigations, the crystal to non equilibrium phase transition induced by ball - milling has been observed in the case of a pure element - Si and in the case of two binary alloys which exhibit a positive heat of mixing - Si/Sn and Si/Zn. The observation of such transition supports the idea that the mechanism of the non - equilibrium phase transition induced by ball - milling has to be distinct from the one leading to the amorphisation by interdiffusion of a multilayered system.

Acknowledgements :

We gratefully acknowledge Dr.A. Quivy for her help in the obtention of the X - ray patterns.

References

/1/ A.Y. Yermakov, Y.Y. Yurchikov, V.A. Barinov
Phys. Met. Metall., 52 (1981) 50

/2/ C.C. Koch, O.B. Cavin, C.G. McKamey, J.O. Scarbourgh
Appl. Phys. Lett., 43 (1983,) 1017

/3/ E. Hellstern, L. Schultz
Proc. 6th Int. Conf. on Rapidly Quenched Metals, Montreal, 1987
Mat Sci. Eng., 97 (1988) 39

/4/ L. Schultz, E. Hellstern, A. Thoma
Europhys. Lett., 3(8) (1987) 921

/5/ E. Gaffet, N. Merk, G. Martin, J. Bigot
J. Less Comm. Met., 145 (1988) 251
/6/ E. Gaffet, N. Merk, G. Martin, J. Bigot
DGM Conf. "New Materials by Mechanical Alloying Techniques"
3 - 5 October 1988, Hirsau - West Germany , 95
Organizers : E. Arzt; L. Schultz
/7/ J. R. Thompson, C. Politis
Europhys. Let., 3(2) (1987) 199
/8/ B. P. Dolgin, M.A. Vanek, T. McGory, D.J. Ham
J. Non Cryst. Sol., 87 (1986) 281
/9/ R.B. Schwarz, C.C. Koch
Appl. Phys. Lett., 49(3) (1986) 146
/10/ M.S. Boldrick, D. Lee, C.N.J. Wagner
J. Less Com. Met., 106 (1988) 60
/11/ C. Politis, W.L. Johnson
J. Appl. Phys., 60(3) (1986) 1147
/12/ A. Hitaka, M.J. McKenna, C. ElBaum
Appl. Phys. Lett., 50(8) (1987) 478
/13/ A. W. Weeber, H. Bakker, F.R. de Boer
Europhys. Lett., 2(6) (1986), 445
/14/ P.Y. Lee, C.C. Koch
Appl. Phys. Lett., 50 (1987) 1578
/15/ N. Merk, E. Gaffet, G. Martin
J. Less Comm. Met., submitted to
/16/ L. Schultz
J. Less Comm. Met., 145 (1988) 233
/17/ E. Gaffet, M. Harmelin
J. Less Com. Met, accepted for publication
/18/ A. Antoniadis, J. Berruyer, A. Filhol
Institute Lauë Langevin internal report (1988) 87AN22T
/19/ Kiendl H.
Zeichrift für Naturfor., 22A(1), 1967, 79
/20/ H.E. Kissinger
J. Res. Nat. Bur. Standards, 57(4), 1956, 217
/21/ S. Veprek, Z. Iqbal, F.-A. Sarott
Phil. Mag. B, 45(1), 1982, 137
/22/ A. G. Cullis, H.C. Webber, N.G. Chew, J.M. Poate, P. Baeri
Phys. Rev. Lett., 49(3), 1982, 219
/23/ R. Bahdra, J. Pearson, P. Okamoto, L. Rehn, M. Grimsditch
Phys. Rev. B, 38(17), 1988, 12656
/24/ Birringer R., Hahn H., Höfler H., Karch J., Gleiter H.
Defect and Diffusion Forum, 59 (1988) 17